The compressed non-uniformity effect of gas diffusion layer on PEMFC performance

P. H. Chi[*a], S. H. Chan[a], F. B. Weng[a], Ay Su[a] and C.Y. Lin[b]

[a]Department of Mechanical Engineering & Fuel Cell Research Center, Yuan Ze University, Chung-Li, Taiwan, R.O.C.

[b]Department of Mechanical Engineering, Nanya Institute of Technology

ABSTRACT

The purpose of the present study is to investigate both experimentally and theoretically the effect of GDL porosity non-uniformity due to clamping force on fuel cell performance. In the experimental study, a unit cell with a single serpentine channel is employed to test the effect of compression force on cell performance. The degree of GDL deformation is achieved by varying the thickness of gasket spacer. In the numerical simulations, a three dimensional model is developed to simulate coupled electrochemical kinetics, current distribution, hydrodynamics, and multi-component transport. The properties of the GDL used in the simulation are expressed as functions of the compression ratio. The simulation results are found to be in good agreement with experimental data in overall fuel cell performance. The distributions of temperature, heat flux, species concentration, current density and saturation are found to be highly oscillating in nature between the local rib and channel locations. Furthermore, the higher the compression ratio, the better is the cell performance and the larger is the fluctuation amplitude. Finally, the higher the compression ratio, the more are the saturation, water flooding and hydrogen deficiency downstream. More detail compression effects on membrane conductivity, etc, are also presented.

Keywords: Gas diffusion layer, deformation, numerical simulation, fuel cells

[*] Corresponding author
Phone: +886-3-4618691, FAX: +886-3-4555574, Email: glixlink@msn.com

1. INTRODUCTION

Performance of proton exchange membrane (PEM) fuel cells is impacted by the properties of the gas diffusion layer which can affect the optimum performance of the catalyst and electrode and, therefore, plays an important role in cell performance [1]. The gas diffusion layer (GDL) used in PEM fuel cells is made of either carbon fiber paper or carbon cloth. Ideally, the GDL has the function of efficiently transporting reactant gases to catalyst layers, removing liquid water to the gas channels, conducting electrons with low resistance, and maintaining low contact resistance at contact interfaces. Such mass transport occurring in the diffusion layer has been shown to have a strong effect on PEM fuel cell performance [2]. In a fuel cell, or stack, the cell components are held together under a high compressive load to prevent gas leakages. Gas leakages cause poor performance and lead to potentially dangerous situations; while over-compressing the GDL increases mass transfer resistance and thus reduces cell performance. High installation pressure can generally decrease the contact resistance and it has been shown that physical compression of the GDL directly increases its electrical conductivity [3]. Most of the studies in this area have assumed, for simplicity, constant porosity of the GDL or, in other words, a uniformly compressed GDL. However, this cannot reflect the important effects on fuel cell performance of variation in GDL porosity, which becomes non-uniform under compression. The following section provides a brief review of related research. Section 2 provides the specifics of the experiment and model development and the results and discussion can be found in section 3 along with recommendations for further research.

Several recent studies have begun to explore the effect on performance of compression on the GDL. Zhou et al. [4] used a two-dimensional model of the rib and GDL to investigate the effect of clamping force on the interfacial contact resistance and the porosity of the gas diffusion layer (GDL) in a proton exchange membrane fuel cell (PEMFC). The numerical results showed that a larger clamping force and wider rib lead to smaller contact resistance. However, the porosity of the GDL was observed to decrease with increasing clamping force. Rectangular-shaped ribs were found to lower the contact resistance and porosity of GDL to a greater degree than semicircular-shaped ribs which was improved fuel cell performance. Lee et al. [5] experimentally investigated cell performance as a function of compression

pressure with different commercial types of gas diffusion layers. Their investigation showed that changes in cell performance may be due to changes in the porosity, the contact resistance of the gas diffusion layer, and the excluded water in the membrane. Further, optimum cell performance was found to depend on the gasket thickness and the degree of compression of the diffusion layer. Ge et al. [6] studied the effects of GDL compression on fuel cell performance for different compression ratios (operating thickness / original thickness) and under different fuel cell operating conditions. They found that an optimal compression ratio exists and that the ratio occurs at the same percentage for different running conditions. However, the value of this ratio was found to change when different types of GDL (such as carbon fiber paper or carbon cloth) were used. Roshandel et al. [7] considered the spatial variation in porosity due to compression pressure and water produced effects. They postulated that a sine wave type porosity distribution exists underneath the landing area (rib) of GDL when a clamping force is applied. Chu et al. [8] used a one-dimensional half-cell model to investigate the effects of non-uniform porosity on fuel cell performance in terms of physical parameters such as oxygen consumption, current density, power density, etc. The non-uniformity of porosity was accounted for by four different continuous functions of position, each of which had a different averaged value of porosity and a different type of distribution across the diffusion layer. Their results showed that fuel cell performance deteriorates significantly due to a lower porosity effect in the GDL as the cathode is flooded with water.

In both of the latter studies (Roshandel et al. [7] and Chu et al. [8]) variable porosity was accounted for, but constant permeability of the GDL was assumed. In recent years, however, the assumption of constant permeability has come under scrutiny and new studies have appeared that tackle the issue of how changes in the permeability of the gas diffusion layer may impact PEM fuel cell performance. Williams et al. [1] experimentally observed that over-land convection could significantly improve cell performance and delay the onset of the mass transfer limiting regime. Ihonen et al. [9] reported that the use of high clamping pressure decreased the permeability of the GDL. J.G. Pharoah [10] used computational fluid dynamics (CFD) to determine the importance of convective transport and how it operates as a function of GDL permeability when beyond a threshold permeability value of approximately $1\times10^{-13}\,m^2$, assuming constant porosity in the GDL.

However, in their recent experimental study, Gostick et al. [11] found that if a GDL is compressed to the half of the initial thickness, its permeability is decreased by an order of magnitude. Thus, all previous research suggests that the compression of the diffusion layer will generally influence not only the conductivity and contact resistance but also the porosity and permeability of the diffusion layer and affect cell water management, as well.

However, compression force is not uniform across the GDL layer due to the rib and channel design of PEM fuel cells. When clamping force is applied, the porosity of areas of the GDL in contact with the ribs of the bipolar plate can be significantly different from areas of the GDL in contact with the channels of the bipolar plate. This difference can give rise to local variation phenomena which can affect the built-in design durability of PEM fuel cells, an important concern in addition to the overall performance of the fuel cell. For instance, a non-uniform temperature distribution can cause thermal stress in the membrane and catalyst layers and a non-uniform saturation distribution can cause local water flooding which can reduce the useful reactive area. Therefore, it is also important to model the effects of non-uniform compression force to fully understand the processes at work in the fuel cell and their implications for performance.

While the text of research discussed in the preceding paragraphs has helped us to understand the separate effects of GDL compression on porosity and permeability and corresponding effects on fuel cell performance, to date no prior numerical studies have considered the effects of variation in both the permeability and porosity of GDL compression, simultaneously. Similarly, no extant studies have utilized a non-uniform model of GDL compression weighed against experimental data to explore which of the models fits best with the empirical data. Thus, the aim of the present study is to investigate the effects of simultaneous variation of permeability and porosity due to GDL compression as well as non-uniform compression model in explaining the experimental results and providing important data about fuel cell processes in GDL compression situations.

More specifically, this study investigates this non-uniform porosity effect for a non-uniform square wave variation model allowing for a smaller porosity under the rib (the compressed part) and for a larger porosity under the flow channel (the uncompressed part). A three dimension numerical simulation analysis is adopted here to better understand local phenomena, such as temperature, current density,

species, saturation (liquid water), and membrane conductivity distributions, in addition to the overall performance of PEM fuel cell. Thus, the specific objectives of this work are to (1) to validate the detailed 3-D numerical PEM fuel cell model through the comparison of fuel performance with experimental results under different compressed ratios of GDL, and (2) to study local phenomena in detail to help explain how different GDL compression ratios affect fuel cell performance.

2. EXPERIMENTAL SETUP AND MODEL DEVELOPMENT

2.1 Experimental Setup

A unit cell is employed to obtain cell performance data under different GDL compression ratios. The hardware of the unit cell, from inside out, consists of a membrane electrode assembly (MEA, which includes catalyst layers, a membrane and GDLs), flow field plates, a heating plate, and end plates, see Fig. 1. Graphite plates with serpentine flow pattern are used as the current collector as well as the flow field plates. The MEA (Gore 5621, GoreTex Fuel Cell Co.) has a reaction area 25 cm^2. For each compression ratio case, a Teflon gasket of known thickness is placed around the active area of the MEA as a spacer to control the deformation of the MEA. Three gaskets with the thickness of 0.256, 0.207 and 0.158 mm respectively are used on both the anode and the cathode sides in the experiments. In the present study the compression ratio (CR) is defined as the ratio of the reduced thickness versus the original thickness,

$$CR = \frac{L - l}{L}, \tag{1}$$

which differs from other researchers, e.g. [12]. The CR value by our definition is proportional to the clamping force and hence the compression pressure. The original thickness (L) of GDL is 0.4mm. Assuming the gasket is the much stiffer than the MEA, the thickness (l) of the compressed GDL is the gasket thickness. The CR values for the 0.256, 0.207 and 0.158 mm gaskets are 36%, 48.3% and 60.5%, respectively.

The dimensions of components and operating conditions are set at Table 1.

A fuel cell test system (ScribnerAssociates, model 850C) is employed to record polarization curves and the high frequency ohm resistance/voltage curve of the test cell. Hydrogen and oxygen at 300 c.c./min. and fully-humidified at 65ºC are used as the fuel and oxidant respectively. The cell temperature is maintained at 70ºC. The

outlet pressure of the anode and the cathode is 1 atm. The anode and cathode flow each enters the unit cell from the top in a counter-flow manner, see Fig. 2.

2.2 Model Development

Most of the literature on CFD model for PEMFC considers GDL of uniform properties, e.g. Djilali[13], Wang[14], etc. Recently Su et al. [14,15] reported a 3D CFD model that considered non-uniform property distributions for the GDL, although the GDL domain did not take into consideration the actual deformation of the material. In the present study the non-uniformly compressed GDL, cf. Fig. 1, which contains compressed parts and uncompressed parts is considered. The porosity of GDL underneath the ribs is decreased by the compression force. Three CR values (36%, 48.3% and 60%) are used in the experiments and numerical simulation for comparison. An addition CR value of 70% is included in the numerical simulation to predict the cell performance under extreme compression conditions.

2.2.1 Assumptions for the Numerical Model

The numerical simulations performed in the present study are based on the solution of the conservation equations of mass, momentum, energy, saturation, current and species transport on a computational grid using finite-volume methodology. The key elements in the modelling of fuel cells are the transport phenomena through porous media, heterogeneous reactions within porous electrodes and the coupling between mass transports, electrochemical reactions and current–potential fields. A commercial CFD software [16], CFD-ACE+ v. 2003, is employed in the present study. The theoretical background and validation of this simulation tool can be found in recent papers by Sui et al[15]. For the 3D simulations performed in the present study, we make the following assumptions:

1. The system reaches a steady state.
2. Laminar flow and ideal gas for the fluids considered.
3. Stefan-Maxwell for multi-component gas diffusion.
4. The electrochemical kinetics is described by the Butler-Volmer equation.
5. Proton transport in the ionomer is described by the Nernst-Planck equation.
6. Negligible contact resistance.
7. The deformation of GDL is elastic.

According to the assumptions, the governing equations corresponding to the various regions of the fuel cell are given below [17]. The simulation code itself has been verified elsewhere [18].

2.2.2 Porous media properties

The thermal conductivity λ is a combination of the porosity, solid and fluid thermal conductivity and is defined by following equation [19, 20],

$$\lambda = -2\lambda_s + \frac{1}{\frac{\varepsilon}{2\lambda_S + \lambda_F} + \frac{1-\varepsilon}{3\lambda_S}} \tag{2}$$

where the λ_S and λ_F are the solid and fluid thermal conductivity, ε is the porosity of the porous media. When $\lambda_S >> \lambda_F$, this reduces to

$$\lambda \sim \frac{2\lambda_S(1+\varepsilon)}{2+\varepsilon} \tag{3}$$

The species diffusivity in the GDL is related to porosity using the Bruggeman relation [20, 21]:

$$D_i = D_{i,FS} \cdot \varepsilon^{\tau} \tag{4}$$

where τ is the tortuosity factor and $D_{i,FS}$ is the free space diffusivity.

2.2.3 Compressed GDL Model

The effect of compression on GDL is assumed to be elastic and the clamping force does not destroy the solid fibbers of the porous media but merely reduces the pores space. The edge effect is neglected for its relatively smaller scale. The porosity of the compressed GDL is closely related to the pore space, which can be readily derived to yield the following equation:

$$\varepsilon_{compressed} = \frac{\varepsilon_{original} - CR}{1 - CR} \tag{5}$$

The absolute permeability (κ) is a function of porosity (ε) and is defined by the Carman-Kozeny equation [22, 23]:

$$\kappa = \frac{D_r^2 \cdot \varepsilon^3}{16 \cdot C_k (1-\varepsilon)^2} \tag{6}$$

where the Kozeny constant $C_k = 6$ and particle diameter $D_r = 7 \times 10^{-6}$.

2.2.4 Computational Domain and Boundary Conditions

The 3D CFD computational model resolves most of the components used in the experiments, i.e. GDLs, catalyst layers, membrane, gas channels and solid bipolar plates. The computational domains are divided into 32 elements in the *X*-direction, 164 elements in the *Y*-direction, and 49 elements in the *Z*-direction. The total number of the simulation model contains 257,152 cells. The grid distribution is found to be adequate for reproduction of simulation results with higher number of cells. At gas inlets, gas composition and mass flow rate is prescribed and at gas outlets the pressure is set to be 1 atm. The temperature boundary condition on both sides of the current collector is set to be constant while the remaining surface of the domain is set to be adiabatic.

3. RESULTS AND DISCUSSION

The properties, parameters and baseline conditions used in the numerical simulations are listed in Table 1 and 2. Three GDL compression cases (CR=36%, 48% and 60%) and parameters for the experiments and numerical simulations are shown in Table 3.

In the follow discussion of simulation results, the distribution of temperature, saturation and current density distributions are presented on a Z-cut plane, cf. Fig.2, through the cathode catalyst layer (CCL), while the membrane electrical conductivity distribution are presented on a Z-cut plane through the membrane layer. The species concentration is presented through the CCL for oxygen and the ACL for hydrogen. In the mean time, we cut the Z-plane (such as CCL, PEM and ACL) and the centre X-plane to yield a Y-Y line along the Y direction, cf. Fig. 2. The data shown along the Y-Y line reveal the variation from the inlet up-stream all the way to the outlet down-stream location. The channel and rib widths are both 0.0012 m. The inlet channel width is located at y axis point 0.0468 m to 0.048 m. The outlet channel width is position at y axis point 0 m to 0.0012 m.

3.1 Comparison of Cell Performance of Simulation and Experiment Data

The experimental data of cell performance and high frequency resistance are shown in Fig. 3. The resistance decreases with increasing compression ratio and the cell performance increases with increasing compression ratio. However, the I-V curves also show that the concentration polarization is affected by CR values, namely,

concentration polarization appears at higher CR cases. This is because at larger CR value, the porosity under the rib tends to decrease; therefore mass transfer limitation is likely resulted therein.

The predicted polarization curves for four CR cases (Sim-36, Sim-48, Sim-60 and Sim-70) are shown in Fig. 4, and are compared with the experimental results at similar conditions except the Sim-70 case of which experimental data are not available. The general trend of predictions agrees well with that seen from experimental data and the agreement appears to be better for the cases with higher CR values. It is noted that the simulated I-V curves extend slightly furthers into the higher current density range such that the simulated concentration polarization begins at the lower voltage value than the experimental value. This can be explained as a result of the step function of non-uniform porosity variation used in the simulation. In the numerical model, the porosity variation is assumed as a step function along the rib-channel direction, namely, only the portion of the GDL immediately under the rib is assumed compressed, whereas in reality the compressed region may extend slightly beyond the edge of the rib. Thus the slightly higher porosity allows for more mass transfer and delays the onset of concentration polarization to a higher current density condition.

3.2 Comparison of different compressed ratio effects

On the basis of the present non-uniform model, effects of different compression ratios (CR) are examined. From the previous IV curves of Fig. 4, it is seen that the higher the CR, the better is the performance in the working voltage range and the earlier is the occurrence of concentration polarization at higher voltages. This is because the higher compression induces less contact resistance, shorter GDL thickness and less pores of GDL to reduce the high frequency resistance and ohmic polarization. Although the less pores of GDL can increase the electric transfer cross section area, it can also reduce the mass transfer of reactants (fuel or oxidant) to or the product (water vapour) released from the catalyst layer. In consequence, the higher CR value reduces the high frequency resistance to improve the performance in the cell working voltage range (0.4~0.65V), and also causes the earlier concentration polarization below the cell working voltage range.

Figure 5 and 6 show the respective normalized distributions from the upstream inlet to the downstream exit along the Y-Y line with different compressed ratio of 36% (Sim-36), and 60% (Sim-60). Substantial difference exists. For 36% CR(E-36N

in fig.5), current density is the lowest but stable, saturation rises from upstream to over 0.2 after rib 13 and then to the maximum value of 0.5 at the downstream exit, membrane conductivity rises up to the maximum after rib 12, and some hydrogen mass fraction remains at exit. For 60% CR, Fig.6 shows that current density is higher than 36% CR value and drops, rather than stable, after rib 10, saturation rises faster and is over 0.2 after rib 9 and 0.6 maximum at exit, membrane conductivity also rises faster to the maximum at rib 10 , and little hydrogen mass fraction remains after channel 15. For even higher CR value of 70%, Fig.5 shows that current density is the highest but drops faster at the further upstream location of rib 9, saturation rises even faster and reaches the maximum of 0.8 at exit, membrane conductivity increases to the maximum after rib 8, and hydrogen mass fraction depleted earlier after channel 13. Thus several conclusions can be reached. (1) The higher the compression ratio, the higher and the faster is the saturation rise along the stream. The finial saturation value at the exit is proportional to the CR value. (2) Similarly, the current density is larger for higher compressed GDL, but drops down at the earlier downstream location due to flooding (saturation). (3) The earlier flooding causes the earlier hydrogen deficiency along the stream. (4) Finally, the electrical conductivity of membrane also increases faster with higher compression.

A more detail direct comparison between the low 36% and high 70% compression ratio effects is shown in Fig.7. Figure 7(a) shows that 36% CR (Sim-36) yields a fairly uniform temperature distribution, but the high 70% CR(Sim-70) in Fig.7(e) produces not only large local temperature oscillation amplitude between neighboring channel and rib locations but also even larger variation between the upstream and downstream locations. Figures 7(b) and (f) compare the saturation distribution in CCL. They clearly show that high CR produces much more liquid water. Figures 7(c) and (g) show that low CR yields an overall uniform current density distribution while the high CR produces a higher upstream but a lower downstream current density distribution due to water flooding. Comparison between Fig.7(d) and (h) shows that hydrogen mass fraction depleted only near the exit in case of low CR, but almost a third of area is depleted and therefore useless in high CR case due to water flooding. In short, the higher the CR, the more saturation occurs at downstream and the less are the temperature, current density and hydrogen at downstream.

4. CONCLUSIONS

The conventional numerical simulation model of PEM fuel cells assumes that the gas diffusion layer (GDL) can be treated as a uniformly compressed layer. The present study argues that a more realistic model of the GDL is as a non-uniformly compressed layer because the installation force compresses mainly on the ribs against the GDL. For each parameter, the performance predicated by each model was evaluated against the experimental data to assess which model fit better with the results. The following major conclusions are made:

The distributions of temperature, heat flux, species concentration, current density and saturation are found to be highly oscillating locally between the rib and channel locations. The higher the compression ratio, the larger is the fluctuation amplitude.

The temperature and hydrogen distributions are fluctuating in the same phase, higher in channel and lower in rib locations. The saturation, heat flux, current density and membrane conductivity also fluctuate in phase but to a lesser degree in fuel cell channels and to a higher degree in rib locations. The saturation fluctuating distribution reveals that the temperature is lower beneath the rib region which causes local condensation and higher saturation. This phenomenon increases membrane conductivity and cell performance. At the same time, however, it can cause water flooding and decrease the cell performance downstream.

The larger the CR, the greater the saturation occurring downstream and the lower the temperature, current density and hydrogen concentration downstream. The larger the CR value (for the range investigated) the higher is the overall total performance, but the resultant water flooding downstream leads to hydrogen deficiency and less effective use of reaction area downstream. Higher CR values yield greater local temperature oscillation and larger overall temperature variation which may impose higher local thermal stresses on membrane and catalyst layers.

REFERENCES

[1] M.V. Williams, E. Begg, L. Bonville, H. Russell Kunz, J.M. Fenton, J. Electrochem. Soc. 151 (8) (2004) A1173–A1180.

[2] B. Thoben, A. Siebke, J. New Mater. Electrochem. Syst. 7 (2004) 12–20.

[3] J. Nordlund, *The anode in the direct methanol fuel cell*, Doctoral Dissertation.

[4] P. Zhou, C.W. Wu, G.J. Ma, J. Power Sources 159 (2006) 1115–1122.

[5] W.K. Lee, C.H. Ho, J.W. Van Zee, M. Murthy, J. Power Sources 84 (1999) 45–51.

[6] Jiabin Ge, Andrew Higier, Hongtan Liu, J. Power Sources 159 (2006) 922–927.

[7] R. Roshandel, B. Farhanieh, E. Saievar-Iranizad, Renewable Energy 30 (2005) 1557-1572.

[8] Hsin-Sen Chu, Chung Yeh, Falin Chen, J. Power Sources 123 (2003) 1-9.

[9] Jari Ihonen, Mikko Mikkola, and Göran Lindbergh, J. Electrochem. Soc., 151 (8) A1152-A1161 (2004)

[10] J.G. Pharoah, J. Power Sources 144 (2005) 77-82

[11] Jeff T. Gostick, Michael W. Fowler, Mark D. Pritzker, Marios A. Ionnidis, Leya M. Behra, J. Power Sources 162 (2006) 228-238

[12] Fang-Bor Weng, Ay Su, Yur-Tsai Lin, Guo-Bin Jung, and Yen-Ming Chen, J**.** of Fuel Cell Science and Technology, Vol. 2, I 3 (2005), pp. 197-201.

[13] Y.M. Ferng,A. Su, Int. J. of Hydrogen Energy, 32 (2007), 4466-4476.

[14] P.K. Sinha, C. Y. Wang, and A. Su, Int. J. of Hydrogen Energy, 32 (2007) 886-894.

[15] P.C. Sui, N. Djilali, J. Power Sources 161 (2006), 294-300

[16] CFD-ACE+ user maanual.

[17] Sandip Mazumder and James Vernon Cole, J. Electrochem. Soc. 150(11), (2003) A1503-1509.

[18] P.H. Chi, Fang-Bor Weng, Ay Su, and S.H. Chan, J**.** of Fuel Cell Science and Technology, Vol. 3, I 3 (2006), pp. 225-365.

[19] V. Gurau, H. Liu, and S. Kakac, AIChE J., 44 (1998), pp. 2410-2422.

[20] Dagan, G., 1989, *Flow and Transport in Porous Formations*, Springer, Berlin

[21] Kaviany, M., 1995, *Principles of Heat Transfer in Porous Media*, second ed., Springer, New York

[22] Bird, R. B., Stewart, W. E., and Lightfoot, E. N., 1960, *Transport Phenomena*, Wiley, New York.

[23] M.M. Tomadakis, T.J. Robertson, J. Compos. Mater. 39 (2005) 163–188.

Notation

CR	:	compression ratio
δ	:	thickness of compressed GDL
L	:	thickness of uncompressed GDL
l	:	spacer gasket thickness
ε	:	porosity
$\varepsilon_{orinigal}$	:	porosity of uncompressed GDL
$\varepsilon_{compressed}$	:	porosity of compressed GDL
κ	:	absolute permeability (m^2)
λ	:	thermal conductivity
λ_S	:	solid thermal conductivity
λ_F		fluid thermal conductivity
τ	:	tortuosity
$D_{i,FS}$	:	the free space diffusivity

Table 1. Base operating conditions for the numerical model & experiment

Channel width	1.2 mm
Rib width	1.2 mm
Channel height	1 mm
GDL thickness	0.4 mm
Catalyst layer thickness	Anode= 0.018 mm, Cathode= 0.026 mm
Membrane thickness	0.035mm
Total reaction area	25 cm^2
Effective diffusivity	Bruggeman,τ=7 for membrane Bruggeman,τ=1.5 for GDL and catalyst layer
Membrane permeability	1.8×10^{-18} m^2
Catalyst layer permeability	1.76×10^{-11} m^2
Membrane porosity	0.28
Catalyst layer porosity	0.4
Transfer coefficient (Tafel constants) at anode	0.5
Concentration dependence at anode	0.5(H_2)
Reference current density at anode	1.0×10^{9} (A/m^3)
Transfer coefficients (Tafel constants) at cathode	1.5
Concentration dependence at cathode	1.0 (O_2)
Reference current density at cathode	1.5×10^{3} (A/m^3)
GDL and catalyst layer conductivity	100 1/Ω m

Table 2. Different cases and corresponding parameters for the numerical model & experiment

	Anode	Cathode
Inlet gases	H_2	O_2
Inlet volume flow rate(cc/min)	300	300
Inlet gases relative humidity (%)	100	100
Inlet temperature(^oC)	65	65
Operating pressure(atm)	1	1
Cell temperature(^oC)	70	70

Table 3 Dimensions, properties and parameters for the numerical model

Case	Gasket thickness (mm)	Compression Ratio (CR, %)	Uncompressed Porosity	Compressed Porosity	Permeability $\times 10^{-12}$
Sim-36	0.256	36.0	0.8	0.69	3.198
Sim-48	0.207	48.3	0.8	0.61	2.091
Sim-60	0.158	60.5	0.8	0.49	1.108
Sim-70	0.120	70.0	0.8**	0.33	0.495
Exp-36	0.256	36.0			
Exp-48	0.207	48.3			
Exp-60	0.158	60.5			

Original GDL thickness =0.4 mm

Sim-xx : Numerical simulation cases with different compressed ratio.

Exp-xx : Experimental cases with different compressed ratio.

** : Permeability of 0.8 porosity is 6.533×10^{-12}

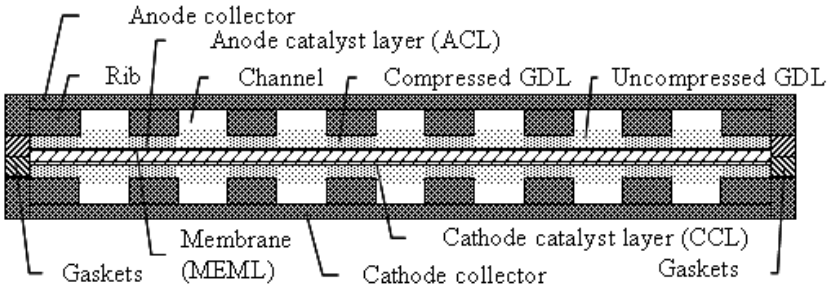

Figure 1. Schematic illustration shows the compressed GDL of PEMFCs

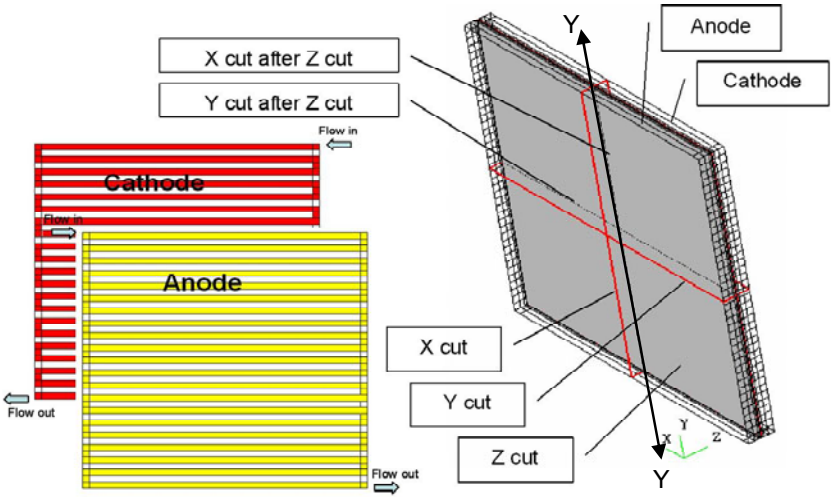

Figure 2 The Z cut plane, X cut plane and line of X cut after Z cut (Y-Y line) are focus domains; and the anode/cathode flow direction

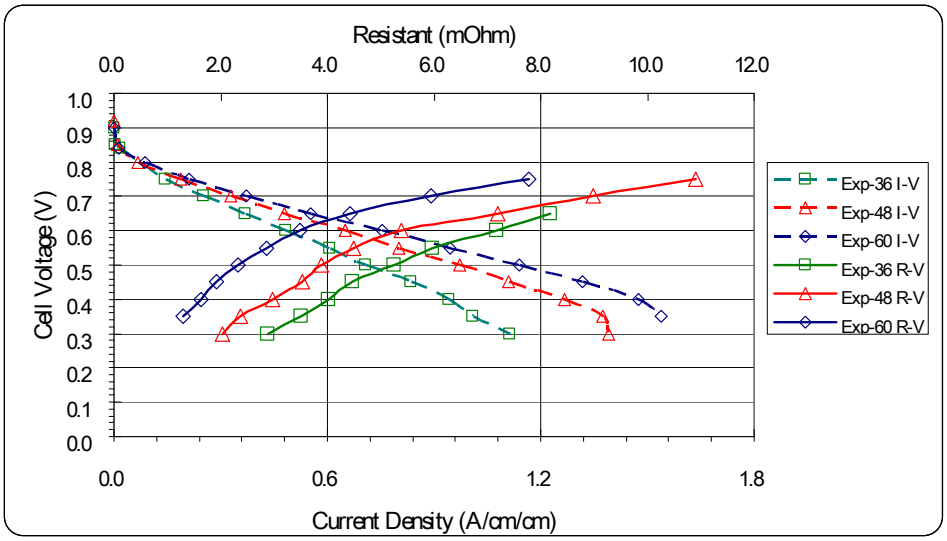

Fig. 3 Experimental data for I-V curve and R-V curve

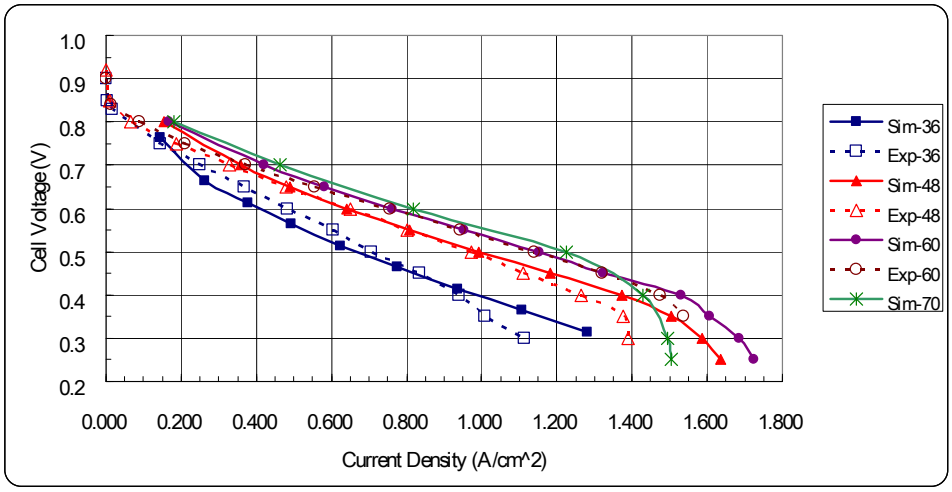

Fig. 4 Polarization curves for different CR value of experiment and simulation data

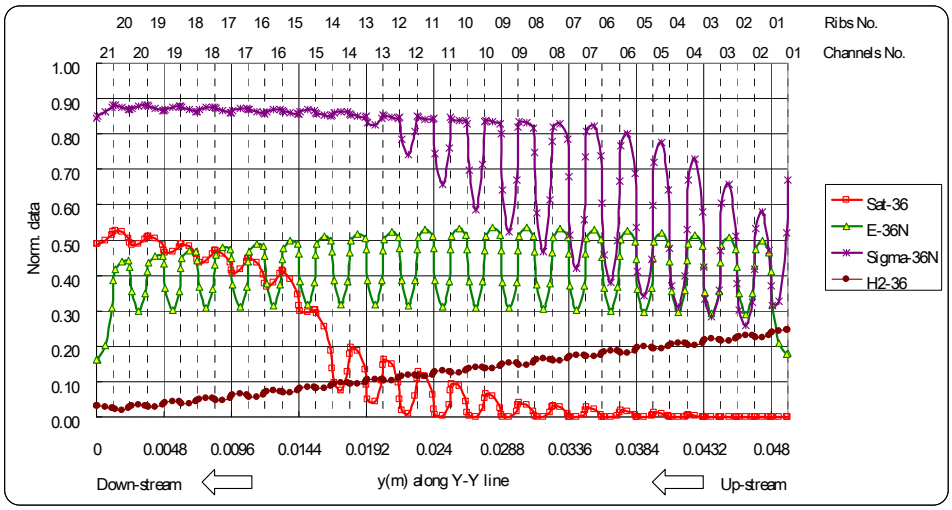

Fig. 5 Normalize data along Y-Y line for different compressed ratio of GDL CR=36% (Sim-36) at operation voltage 0.3V.

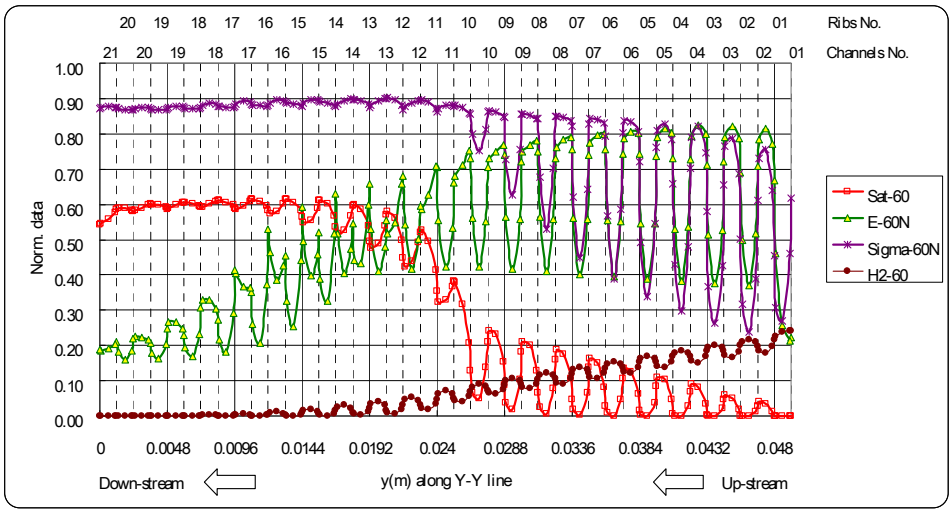

Fig. 6 Normalize data along Y-Y line for different compressed ratio of GDL CR=60% (Sim-60) at operation voltage 0.3V.

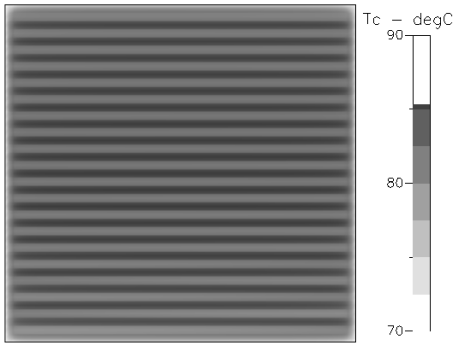

(a) Temperature of Sim-36 at ccl

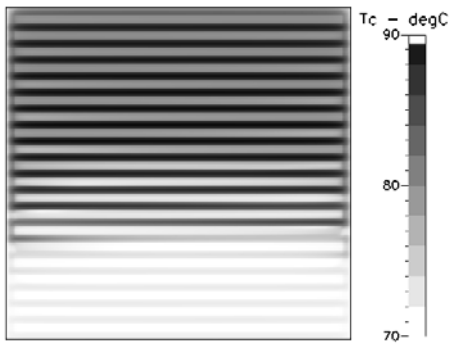

(e) Temperature of Sim-70 at ccl

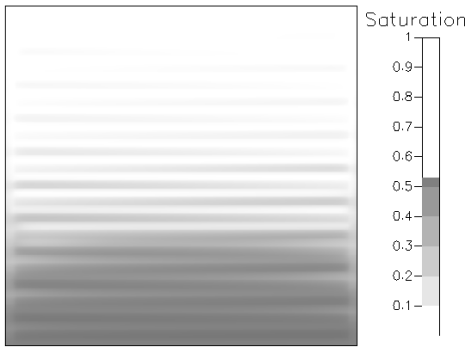

(b) Saturation of Sim-36 at ccl

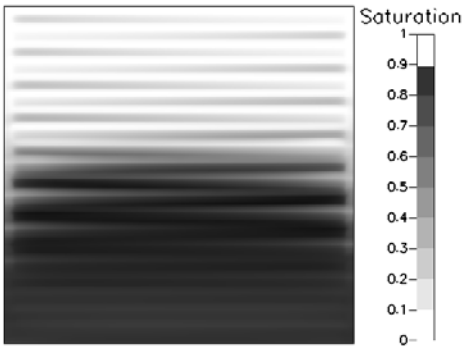

(f) Saturation of Sim-70 at ccl

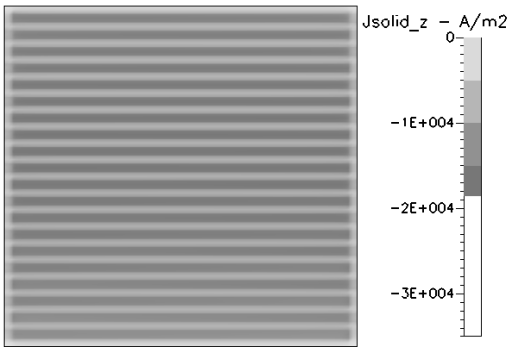

(c) Current density of Sim-36 at ccl

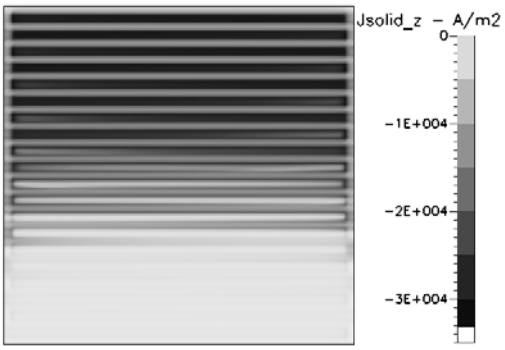

(g) Current density of Sim-70 at ccl

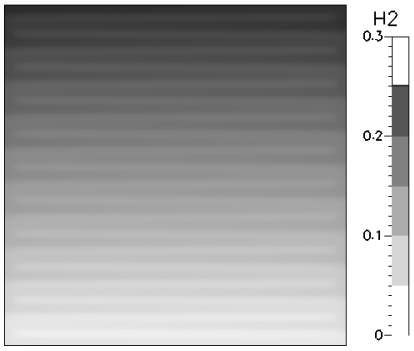

(d) Hydrogen of Sim-36 at acl

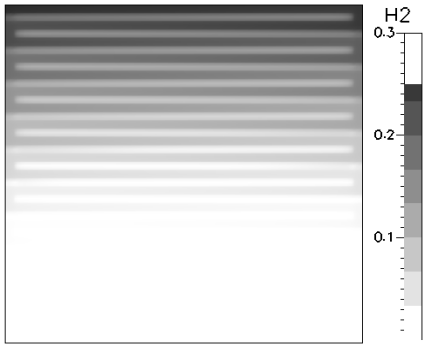

(h) Hydrogen of Sim-70 at acl

Fig. 7 Compare the saturation, temperature, current density and hydrogen mass fraction of Sim-36 ((a1), (b1), (c1) and (d1)) and Sim-70 ((a2), (b2), (c2) and (d2)) at cell voltage of 0.3V.